EXTENDING THE TURBULENT LENGTH SCALE EQUATION WITH THE USE OF LES DATA

UCHECHUKWU S. AGBOGWU[1], EKATERINA K. GUSEVA[2] AND ROLF RADESPIEL[3]

[1]Technische Universität Braunschweig
38106, Braunschweig, Germany
u.agbogwu@tu-braunschweig.de

[2]Peter the Great St. Petersburg Polytechnic University
St. Petersburg, 195220
katia.guseva@inbox.ru

[3] Technische Universität Braunschweig
38106, Braunschweig, Germany
r.radespiel@tu-braunschweig.de

Key words: Turbulence Modelling, Computational Fluid Dynamics.

Abstract. The $k - kL$ closure model naturally occurring higher derivative terms, and due to its nature provides a good starting point for studying effects of inflectional instabilities in wakes. In this work, results of scale resolving simulations of a turbulent boundary layer and its corresponding wake at adverse pressure gradients are evaluated with the aim of establishing physics based bounds and assumptions for the expansion of turbulent length scale equations to improve RANS predictive capability for adverse pressure gradients.

1 INTRODUCTION

The trend in improvement of state of the art transport aircraft is to simplify current design to reduce mechanical complexity, weight and maintenance costs [1,2]. One of the hurdles in the design of high-lift systems lies in the reduced predictive capability of RANS based computational flow models near maximum lift. Critical flow features to be observed include: a turbulent boundary layer, the wake flow of elements located upstream and the confluent flow of upstream element wakes and boundary layers, all subjected to a strong adverse pressure gradient [3,4].

It is important to study wake flows at adverse pressure gradients for several reasons. One is the potential loss of lift of a high lift system due to the flow reversal induced when the wake encounters the adverse pressure gradient created by a downstream element. Recent work indicates that present eddy viscosity based RANS models and Reynolds Stress Models (RSM) significantly under predict the tendency for flow reversal due to adverse pressure gradients observed in experiments [5,6,7]. Secondly, due to the similarities in the characteristics of wake flows and the outer part of turbulent boundary layer flows, a study of wake flows is expected to reveal general mechanisms of shear flows when subjected to adverse pressure gradients. RANS models were originally calibrated to represent typical behaviour of wall bounded flows,

https://doi.org/10.24355/dbbs.084-202003091214-1

near wall damping, log-law of the wall, and to a limited extent, the effect of strong pressure gradients (on wall bounded flows). The spreading rates of self-similar shear flows are usually considered for the model calibration in free shear layers. In [8], a reasonable agreement between $k-\varepsilon$ RANS, RSM and experimental data for wake flows subjected to zero pressure gradient is reported. In adverse pressure gradients, however, both RSM based and eddy viscosity based RANS models under predict the tendency for flow reversal [5,6]. Even though RSM models show better agreement with the experimental data, the role of modelling details is unclear. To be able to improve the predictive ability of RANS turbulence models for adverse pressure gradients, it is possible to consider, among others, the pressure gradient and the corresponding streamwise flow deceleration along with the resulting vortex stretching, inhomogeneity and inflectional instability in the free shear layer, and the mean streamline curvature. The focus of this work is the consideration of the effects of inhomogeneity and the inflectional instability in the free shear layer.

The $k-kL$ model of Rotta [9] provides a good starting point for this purpose. This equation uses an exact transport equation for the turbulent length scale, L and is suited to a term by term modelling [10]. This model naturally includes higher order velocity derivatives, due to a Taylor series expansion of the source term of the length-scale determining equation. In the original derivation of this equation in [9], the second derivative is excluded, with the justification that this term is zero in close-to homogeneous shear flows. Menter and Egorov in [11] argue that the exclusion of the second derivative of the mean velocity is not consistent with the nature of the term, and that the $k-kL$ model loses its superiority over other eddy viscosity based models when no higher order derivative terms are included. Another issue concerns the third velocity derivative from a numerical point of view, as this derivative is hardly included in CFD codes due to difficulties in its numerical approximation.

Based on the availability of instantaneous field values from experiments and results of high-fidelity Scale-Resolving Simulations (SRS), it is possible to first revisit the $k-kL$ equation, including both the second and third mean velocity derivatives in the source terms for a turbulent boundary layer flow and its corresponding wake subjected to adverse pressure gradients. With SRS data it is possible to compute correlation tensors, which will be shown to be instrumental in comparing the contributions of individual velocity gradient terms to the total source term of the kL – transport equation. Information derived from the study of this source term will provide first insight into how the kL length scale determining equation may be extended for the flow case under consideration.

The rest of the paper is as follows: in Section 2 a brief description is given of the computational problem statement and numerical aspects of the SRS of a wake subjected to APG. Rotta's derivation of the kL equation is briefly introduced and the term to be investigated is highlighted in Sections 3 and 4. Finally, conclusions are drawn based on the present results, particularly regarding how best to proceed with the extension of the model.

2 NUMERICAL EXPERIMENTS

This setup for SRS, namely, zonal RANS-IDDES, computations is based on the experimental flow model designed and manufactured in the Technische Universität Braunschweig (TU BS). Its detailed description along with an outline of the experimental setup is presented in [12]. Figure 1 shows a sketch of the experimental flow model which includes a

https://doi.org/10.24355/dbbs.084-202003091214-1

flat plate (FP) as a wake generator and two pairs of symmetrically installed liner foils (LF1 and LF2) creating the adverse pressure gradient, APG. The level of the created APG may be controlled by varying the distance of the upper and lower liner foils to the center plane of the test section.

In the experiments the free stream velocity U_∞ is varied from 24m/s to 48m/s. This corresponds to the variation of the Reynolds number based on the plate length L = 1.058 m and U_∞ from 1.6 to 3.2 million (simulations were performed for both Re = 1.6 and 3.2 million). Corresponding Mach number is less than 0.1, which justifies using the incompressible flow assumption in the simulations.

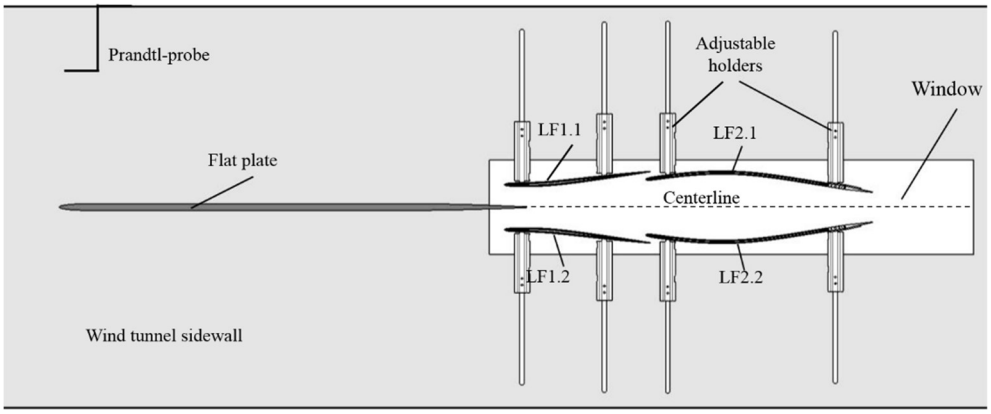

Figure 1: Sketch of experimental flow model installed in wind tunnel used for experiments

The computational domain and grid in *XY*-plane used in the simulations are shown in Figure 2. The entire computational domain is subdivided into two sub-domains (zones); a RANS zone and an IDDES zone. In the RANS zone the *k*- ω RANS model of Menter [13] is applied, whereas in the IDDES zone, the IDDES approach in [14] is used, with the same underlying RANS model. The RANS zone extends from the inlet boundary of the domain to the section x = -0.3m and includes the outer part of computational domain at larger x and boundary layers forming on the liner foils. The IDDES zone covers the rest (downstream) of the flat plate boundary layer and the wake. To ensure rapid transition from modelled turbulence in RANS domain to partly resolved turbulence in the IDDES domain, the Volume Synthetic Turbulence Generator (VSTG) [15, 16] was used at the RANS-IDDES interface. Hence, in the downstream part of the attached FP boundary layer the IDDES performs as Wall Modelled LES (WMLES) and in the wake it functions as a pure LES [14].

On the flat plate and liner foil surfaces no-slip conditions were applied. At the inflow, uniform profiles of all the flow quantities except for the pressure were specified, and at the outflow boundary a constant pressure was imposed. The upper and lower boundaries were treated as slip walls, and in the spanwise direction periodic boundary conditions were imposed, which assumes the 2D mean flow character in the experiment. The span size of the domain was set equal to 0.1m (this was found to be sufficient to ensure span-size independent statistical flow characteristics).

https://doi.org/10.24355/dbbs.084-202003091214-1

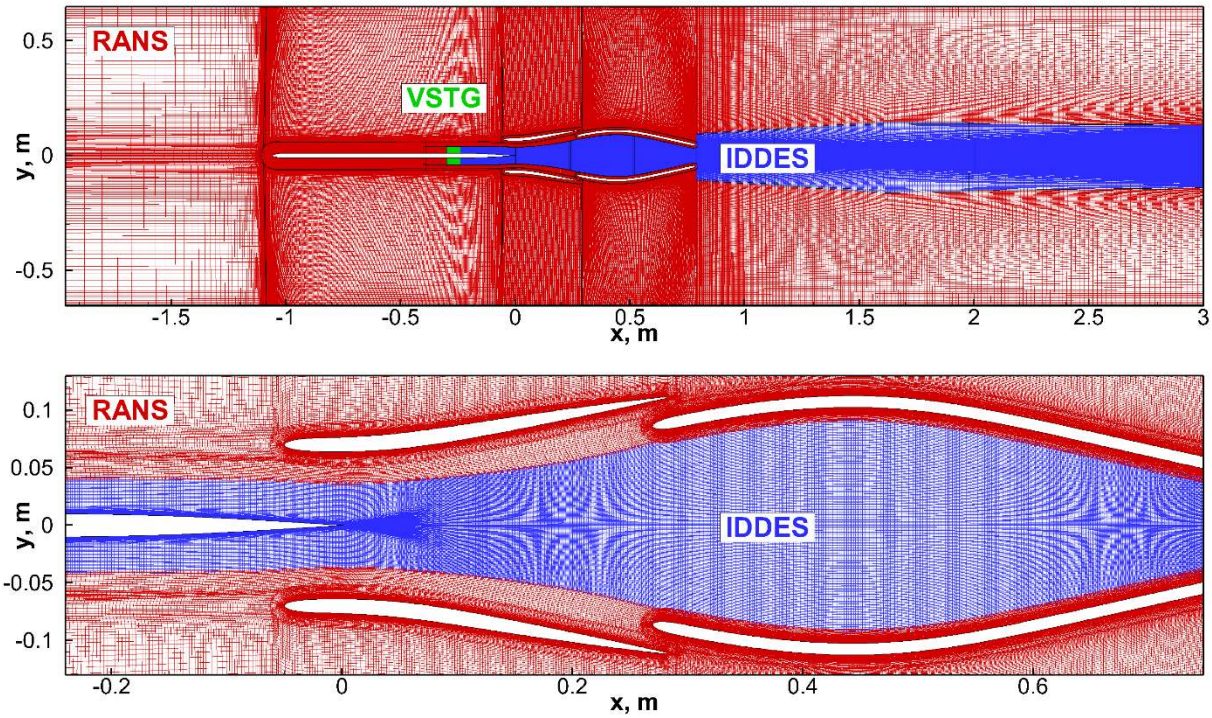

Figure 2: Computational domain, grid, and RANS & IDDES sub-domains in XY-plane. Upper frame: full domain; lower frame: zoomed in wake region

Simulations were performed on a structured Chimera-type grid containing 22 overlapping blocks with around 30M cells total. The grid is clustered near the flat plates and liner foil walls so that the size of the first near wall step in the wall-normal direction would be less than 1.0 in wall units. In the IDDES sub-domain the grid steps in the streamwise and spanwise directions, Δx and Δz, are equal to $2 \cdot 10^{-3}$m and 10^{-3}m, respectively, which corresponds to $\Delta x/\delta = 0.15$, $\Delta z/\delta = 0.075$ (δ is the thickness of the boundary layer in the vicinity of the FP trailing edge). These steps were proven to be sufficiently small for obtaining nearly grid-independent solution [17].

The computations were performed with the use of the in-house code of the Saint-Petersburg Polytechnic University "Numerical Turbulence Simulation" (NTS code) [18]. This is a cell-vertex finite-volume code accepting structured multi-block overset grids of the Chimera type. The incompressible branch of the code used in the simulations employs the flux-difference splitting method of Rogers and Kwak [19]. In the RANS sub-domain, the inviscid fluxes in the governing equations are approximated with the use of a 3rd-order upwind-biased scheme and in the IDDES sub-domain a 4th-order central scheme is used. The viscous fluxes are approximated with the 2nd-order central scheme. For the time integration, an implicit 2nd-order backward Euler scheme with sub-iterations is applied. The time step Δt was chosen to ensure less than 1.0 Courant number.

Figure 3 presents flow visualization in the form of instantaneous isosurface of the Q-criterion coloured by streamwise velocity (liner foils are not shown). The figure visibly displays fine resolved turbulent structures in the IDDES sub-domain (both in the attached FP boundary layer and in the wake), thus suggesting a plausible functionality of the zonal RANS-IDDES approach.

https://doi.org/10.24355/dbbs.084-202003091214-1

Other than that, the flow visualizations clearly reveal the presence of an extended stagnation region in the wake, which is a peculiar feature of the wakes subjected to APG.

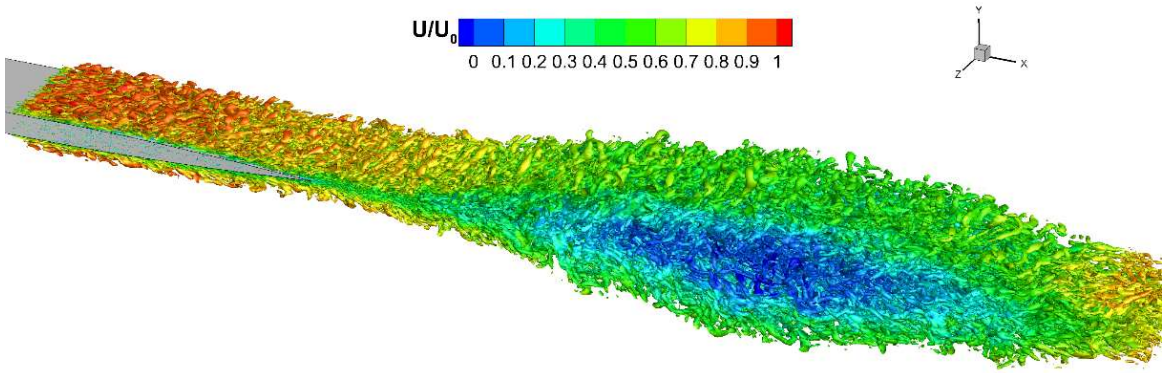

Figure 3. Isosurface of Q-criterion coloured by streamwise velocity

3 THE $k-kL$ EQUATION

3.1 Derivation

Beginning with a simplified transport equation for the diagonal of the two-point spatial correlation tensor, R_{ii}, for a simple shear flow, where

$$\boldsymbol{R}_{ij} = \overline{u_i'(\boldsymbol{x})u_j'(\boldsymbol{x}+r_y)} \tag{1}$$

and defining L as

$$kL = \frac{3}{16}\int_{-\infty}^{\infty} \boldsymbol{R}_{ii}(\boldsymbol{x}, r_y)\, dr_y \tag{2}$$

where k is the turbulent kinetic energy, Rotta derives a transport equation for kL as

$$\begin{aligned}
&\overbrace{\bar{u}\frac{\partial(kL)}{\partial x} + \bar{v}\frac{\partial(kL)}{\partial y} + \frac{3}{16}\int_{-\infty}^{\infty}\left[\frac{\partial\bar{u}(\boldsymbol{x}+r_y)}{\partial x} - \frac{\partial\bar{u}(\boldsymbol{x})}{\partial x}\right]R_{ii}\, dr_y}^{\text{Convection}} \\
&+\overbrace{\frac{3}{16}\frac{\partial\bar{u}(\boldsymbol{x})}{\partial y}\int_{-\infty}^{\infty}R_{21}\, dr_y + \frac{3}{16}\int_{-\infty}^{\infty}\frac{\partial\bar{u}(\boldsymbol{x}+r_y)}{\partial y}R_{12}dr_y}^{\text{Production}} \\
&\overbrace{-\frac{3}{16}\int_{-\infty}^{\infty}\frac{\partial}{\partial \boldsymbol{r_y}}\left(R_{(ik)i} - R_{i(ik)}\right)dr_y - \nu\frac{3}{8}\frac{\partial^2 R_{ii}}{\partial r_k \partial r_k}}^{\text{Dissipation}} \\
&\overbrace{+\frac{\partial}{\partial y}\left\{\frac{3}{16}\int_{-\infty}^{\infty}\left[R_{(i2}{}_{i} + \frac{1}{\rho}\left(\overline{p'v'} + \overline{v'p'}\right)\right]d\, r_y - \nu\frac{\partial(kL)}{\partial y}\right\}}^{\text{Diffusion}} = 0
\end{aligned} \tag{3}$$

The integral part of the convection term is ignored, as the change of $\bar{u}$ in the x- direction is considered negligible. The terms containing the viscosity are considered negligible based on

https://doi.org/10.24355/dbbs.084-202003091214-1

the assumption of a sufficiently high Reynolds number. The diffusion and dissipation terms are modelled using a gradient diffusion model and dimensional arguments respectively. The focus is on the second part of the production term.

Applying a Taylor series expansion on this term, one arrives at

$$P_{kL} = \frac{3}{16}\frac{\partial \bar{u}(\boldsymbol{x})}{\partial y}\int_{-\infty}^{\infty} R_{21}\, dr_y + \frac{3}{16}\frac{\partial \bar{u}(\boldsymbol{x})}{\partial y}\int_{-\infty}^{\infty} R_{12}\, dr_y + \frac{3}{16}\frac{\partial^2 \bar{u}(\boldsymbol{x})}{\partial y^2}\int_{-\infty}^{\infty} r_y R_{12}\, dr_y + \frac{3}{16}\frac{\partial^3 \bar{u}\,(\boldsymbol{x})}{\partial y^3}\int_{-\infty}^{\infty} r_y^2\, R_{12} dr_y + \mathcal{O}\left(r_y^3\right) \tag{4}$$

This term is the focus of interest of the present work. Given available LES data, the total term may be computed and the individual contributions of individual gradient terms can be extracted. This provides insight to what the leading terms may be.

Length scales of production, $L_{12,1}$ and $L_{12,n}$, are defined according to Rotta [9] as shown in equation 5.

$$L_{12,1} = \frac{1}{\overline{u_1' u_2'}}\frac{3}{16}\int_{-\infty}^{\infty}(R_{12} + R_{21})dr_y\,,$$
$$L_{12,n} = \left[\frac{1}{(n-1)!}\frac{1}{\overline{u_1' u_2'}}\frac{3}{16}\int_{-\infty}^{\infty} R_{12} r_y^{n-1}\, dr_y\right]^{1/n} \tag{5}$$

For the purpose of modelling, $L_{12,1}$, $L_{12,2}$ and $L_{12,3}$ are related to the integral length scale, L (which is defined in equation 2) using;

$$L_{12,1} = \zeta_1 L$$
$$L_{12,2}^2 = \zeta_2 L^2 \tag{6}$$
$$L_{12,3}^3 = \zeta_3 L^3$$

Based on the above, the kL transport equation is written in a general form (including the second and third derivatives) as:

$$\frac{\partial (kL)}{\partial t} + \bar{u}_j\frac{\partial (kL)}{\partial x_j} = -\overline{u_i' u_j'}\left(\zeta_1 L\frac{\partial u}{\partial y} + \zeta_2 L^2\frac{\partial^2 u}{\partial y^2} + \zeta_3 L^3\frac{\partial^3 u}{\partial y^3}\right) - \zeta_4 k^{3/2} + \frac{\partial}{\partial x_j}\left[\frac{\nu_t}{\sigma_{kL}}\frac{\partial (kL)}{\partial x_j}\right] \tag{7}$$

3.2 The Production Term

2300 snapshots of instantaneous velocity values from LES computations were used to investigate the contribution of individual derivative terms to the total production term, P_{kL} shown in equation 4. Sections at $x = -0.04m$, representing the turbulent boundary layer and $x = 0.10m$ representing the wake were selected. In case of the turbulent boundary layer with near-wall modelled turbulence we note that fully turbulent flow is obtained for y+>100. Figure 4 shows the results obtained at the two sections. In the section representing the turbulent boundary layer, one can see that the second and third derivative terms contribute less overall to the production term than the first derivative. However, the behaviour of the third term contribution has a higher value near the wall and tends towards zero, in the outer flow region.

In the wake flow, however, while contribution of the second and third terms to the overall source term is limited, the second derivative term tends to become more relevant towards the

https://doi.org/10.24355/dbbs.084-202003091214-1

centreline of the wake. We also note that the total number of LES sample is still only 2400, which appears to be the origin of the asymmetrical distributions observed around the wake centre.

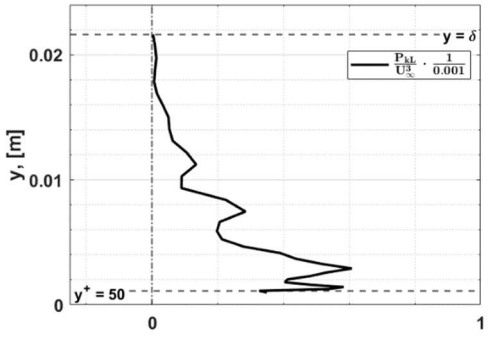

(a) $P_{kL}, x = -0.04m$

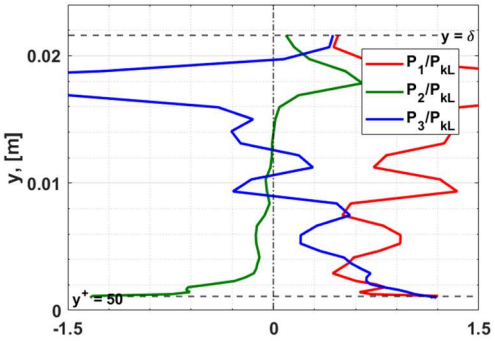

(b) $Production\ Contributions, x = -0.04m$

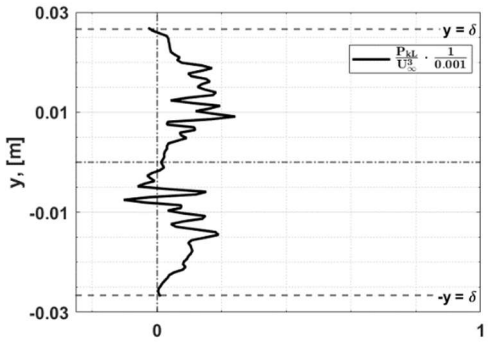

(c) $P_{kL}, x = 0.10m$

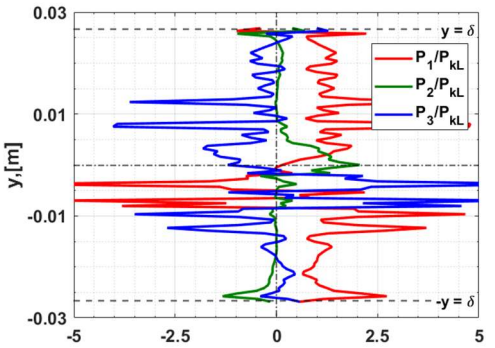

(d) $Production\ Contributions, x = 0.10m$

Figure 4: Total production of kL and corresponding contributions of individual gradient terms

3.3 The Integral Lengths

Using dimensional analysis, the integral length L may also be defined as [20]:

$$L = \frac{C_\mu k^{3/2}}{\varepsilon} \tag{8}$$

where ε is the dissipation and C_μ is a scaling constant equal to 0.09. At the selected positions, the values of L (displayed as L_r, for L as defined in equation 2, and L_ε for L provided in equation 8) are plotted in Figure 5. The values used in L_ε are computed from the averaged LES fields.

An important observation is the need for an additional scaling term. While the relationship between the turbulence variables still holds, it is proposed that the scaling parameters be slightly modified. Here, the relation in 8 was scaled by $C_\mu^{-\alpha}$ where $\alpha = 0.5$. This value was selected empirically. A proposed relation between L and ε is shown in equation 8a. In the conversion of the kL transport equation to the ω transport equation, the parameter C_μ^{α} is included.

https://doi.org/10.24355/dbbs.084-202003091214-1

$$L = \frac{C_\mu k^{3/2}}{C_\mu^\alpha \varepsilon} \tag{8a}$$

3.4 ζ_{1-3}

The plots of ζ_{1-3} are shown in Figure 6. While ζ_1 shows an approximately similar value in both cases, and is similar to that which was obtained in the original work [9], the same may not be said for ζ_3. It is possible to attribute the difference in value of ζ_2 to insufficient samples, but in the former case, the difference of the values between the flat plate and wake is significant enough to suggest that this value may depend on additional information.

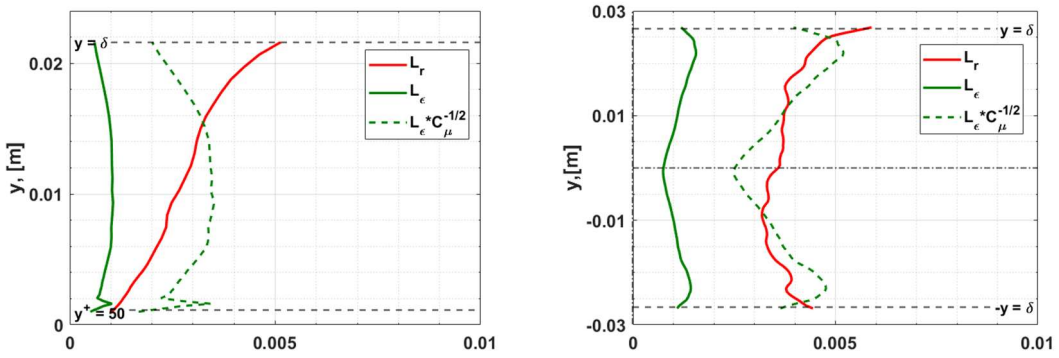

(a) $L, (m)\ at\ x\ =\ -0.04m$ (b) $L, (m)\ at\ x\ =\ 0.10m$

Figure 5: Computed turbulent length scales; the dotted lines show the values when an additional scaling parameter is included

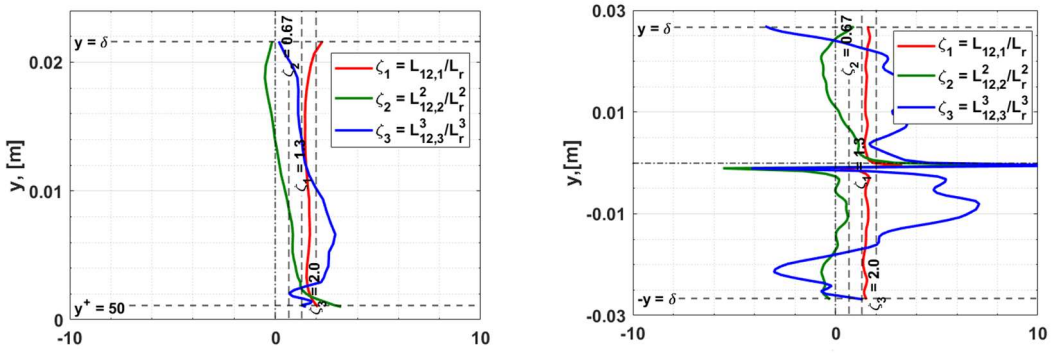

(a) $\zeta_{1-3}\ at\ x = -0.04m$ (b) $\zeta_{1-3}\ at\ x\ =\ 0.10m$

Figure 6: Estimated values of ζ_{1-3}

4 THE ω PRODUCTION TERM

Based on dimensional analysis, the relationship between ω and kL is written as shown in equation 9. From this, the total derivative of ω can be written as shown in equation 10.

https://doi.org/10.24355/dbbs.084-202003091214-1

$$kL = \frac{1}{C_\mu^\alpha}\frac{k^{3/2}}{\omega} \tag{9}$$

$$\frac{D\omega}{Dt} = \left[\frac{3}{2}(kL)\sqrt{k}\frac{Dk}{Dt} - k^{3/2}\frac{D(kL)}{Dt}\right]\frac{1}{(kL)^2 C_\mu^\alpha} \tag{10}$$

From an expansion of equation 10, the omega production term, P_ω, is then written as shown in equation 11.

$$P_\omega = \frac{3}{2}\frac{1}{C_\mu^\alpha}\frac{P_k}{\sqrt{k}L} - \frac{1}{C_\mu^\alpha}\frac{P_{kL}}{\sqrt{k}L^2} = \frac{3}{2}\frac{\omega}{k}P_k - \frac{\omega}{k}\frac{P_{kL}}{L} \tag{11}$$

Where P_{kL} is as defined in either of equations 5 or 7 and P_k is the production term of the k −equation (equation 12).

$$P_k = -\overline{u_i{}' u_j{}'}\frac{\partial \overline{u_i}}{\partial x_j} \tag{12}$$

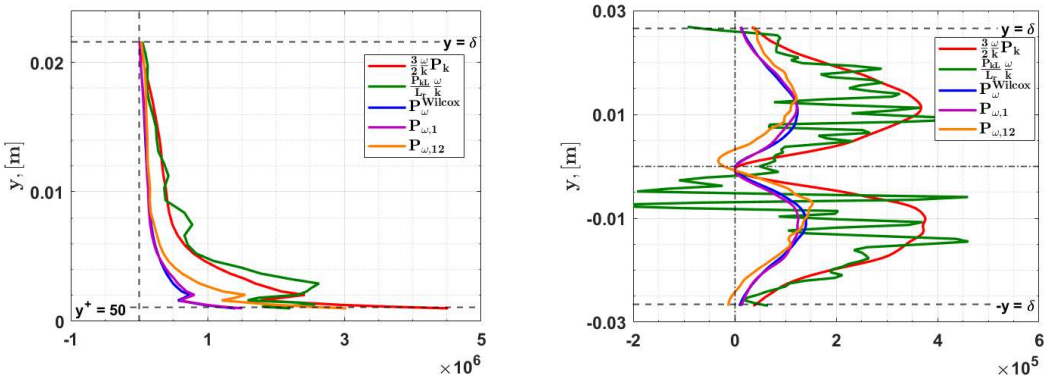

(a) *Contributions to* P_ω *,* $x = -0.04m$ (b) *Contributions to* P_ω *,* $x = 0.10m$

Figure 7: Contributions of different terms to the production of ω. P_ω^{Wilcox}, $P_{\omega,1}$ and $P_{\omega,12}$ are defined in Equations 13, 14 and 15 respectively.

From the graphs shown above, the value of P_ω is expected to be negative, which is unphysical.

$$P_\omega^{Wilcox} = \gamma P_k \frac{\omega}{k} \tag{13}$$

$$P_{\omega,1} = P_k \frac{\omega}{k}\left(\frac{3}{2} - \zeta_1\right) \tag{14}$$

$$P_{\omega,12} = P_k \frac{\omega}{k}\left(\frac{3}{2} - \zeta_1\right) + \zeta_2 L \frac{\omega}{k}\overline{u_i{}' u_j{}'}\frac{\partial^2 \overline{u_i}}{\partial x_j^2} \tag{15}$$

For more insight, this value was plotted using an existing ω transport equation, whose production term contains a simple constant, the Wilcox $k-\omega$ equation. In this equation, $\gamma = 13/25$. From this, it was quickly observed that the value of ζ_1 needs to be kept below 1.5, to

https://doi.org/10.24355/dbbs.084-202003091214-1

ensure that on conversion to the $k-\omega$ from $k-kL$ equation, one is able to maintain a first derivative term that is positive. That is difficult to attain here, as the non-modelled terms will contain values greater than 1.5 at certain points. However, in the above computation of $P_{\omega,1}$, this value was set to 1.0. An estimate of $\zeta_2$was also made at 0.67 and fed into the equation in $P_{\omega,12}$. The same problem previously identified in which the non-modelled terms contain numerical instabilities would have been encountered here, had the non-modelled length scale been implemented. The third coefficient behaves differently in the flat-plate and in the wake, as such no rough prior estimate is possible to make at this stage. Nonetheless, one is able to observe that implementing just the first derivative term produces a similar value to that obtained in the $k-\omega$ Wilcox model. Including the second derivative produces different outcomes. While the production of ω increases towards the wall in the boundary layer flow, in the wake, the production of ω reduces towards the centreline.

4 CONCLUSIONS

The production term of the kL transport equation of Rotta [9] was investigated. It was observed that the third derivative term contributed to the production on the flat plate, while in around the centreline in the wake, the second derivative term appears to contribute significantly to the production of kL. Another important result at this stage is that prior estimates of two coefficients were established, with a physical bound for the first coefficient added.

It is to note, however, that only two arbitrarily selected positions on the flat plate and in the near wake have been considered so far. Additionally, the numerical noise in the computations is expected to be reduced, provided more data is made available for the analysis.

Acknowledgements
The study was funded by DFG and RBRF (Grants No. RA 595/26-1 and No. 17-58-12002). RANS-IDDES computations were performed with the use of resources of the Supercomputer Center “Polytechnichesky” based in Saint-Petersburg Polytechnic University.

REFERENCES

[1] Rudolph, Peter KC. "High-lift Systems on Commercial Subsonic Airliners." (1996).
[2] van Dam, C.P. The aerodynamic design of multi-element high-lift systems for transport airplanes. *Progress in Aerospace Sciences,* (2002). **38**(2):101 – 144.
[3] Rumsey, C. L. and Ying, S. X. Prediction of high lift: review of present CFD capability. *Progress in Aerospace Sciences*, (2002). **38**(2):145 – 180.
[4] Ying S. X., Spaid, F.W., McGinley, C. B., and Rumsey, C. L. Investigation of confluent boundary layers in high-lift flows. *Journal of Aircraft*, (1999). **36**(3):550–562.
[5] Tummers, M.J., Hanjalic, K., Passchier, D.M., and Henkes, R.A.W.M. Computations of a turbulent wake in a strong adverse pressure gradient. *International Journal of Heat and Fluid Flow*, (2007). **28**(3):418 – 428.
[6] Driver, D.M. and Mateer, G. G. Wake flow in adverse pressure gradient. *International Journal of Heat and Fluid Flow*, (2002) **23**(5):564 – 571.
[7] Tummers, M.J., Passchier, D.M., and Bakker, P.G. Experiments on the turbulent wake of a flat plate in a strong adverse pressure gradient. International Journal of Heat and Fluid Flow,

https://doi.org/10.24355/dbbs.084-202003091214-1

(2007) **28**(1):145 – 160. The International Conference on Heat Transfer and Fluid Flow in Microscale (HTFFM-05).

[8] Sugavanam, A. *Near-wake computations with Reynolds stress models*.

[9] Rotta, J.C. *Turbulente Stroemungen*. Vieweg Teubner Verlag, 1972.

[10] Menter, F., Egorov, Y., and Rusch, D. Steady and unsteady flow modelling using the $k-\sqrt{k}L$ model. pages 403–406, 01 2006.

[11] Menter, F.R. and Egorov, Y. The scale-adaptive simulation method for unsteady turbulent flow predictions. Part 1: Theory and model description. Flow, Turbulence and Combustion (2010), **85**(1):113–138.

[12] Breitenstein, W., Scholz, P., Radespiel R., Burnazzi M, Knopp T., Guseva E., Shur M., and Strelets, M. 2019. A Wind Tunnel Experiment for Symmetric Wakes in Adverse Pressure Gradients. AIAA 2019-1875.

[13] Menter, F.R. 1994. Two-Equation Eddy-Viscosity Turbulence Models for Engineering Applications. A*IAA Journal*, **32**, 1598–1605.

[14] Shur, M.L., Spalart, P.R., Strelets, M.Kh, Travin, A.K. 2008. A hybrid RANS-LES approach with delayed-DES and wall-modelled LES capabilities. *Int. J. Heat and Fluid Flow*, **29**, 1638-1649.

[15] Shur, M.L., Spalart, P.R., Strelets, M.Kh, Travin, A.K. 2014. Synthetic Turbulence Generators for RANS-LES Interfaces in Zonal Simulations of Aerodynamic and Aeroacoustic Problems. *Flow, Turbulence and Combustion*, **93**, 63-92.

[16] Shur, M., Strelets, M., Travin, A. 2017. Acoustically adapted versions of STG. *Notes Num. Fluid Mech. and Multidisciplinary Design*, **134**, 62-69.

[17] Guseva E.K., Strelets M.Kh., Travin A.K., Burnazzi M. and Knopp T. 2018. Zonal RANS-IDDES and RANS computations of turbulent wake exposed to adverse pressure gradient. *J. Phys.: Conf. Ser.*, **1135**, 012092.

[18] Shur, M., Strelets, M., and Travin, A., High-order implicit multi-block Navier-Stokes code: Ten-years' experience of application to RANS/DES/LES/DNS of turbulent flows. https://cfd.spbstu.ru/agabaruk/doc/NTS_code.pdf

[19] Rogers S. E., and Kwak D. 1991. An upwind differencing scheme for the incompressible Navier-Stokes equations. *Appl. Numer. Math.*, **8**, 43–64.

[20] Wilcox, D. C et al. *Turbulence modeling for CFD*, volume 2. DCW industries La Canada, CA, 1998.

https://doi.org/10.24355/dbbs.084-202003091214-1